Title
Atmospheric teleconnection mechanisms of extratropical North Atlantic SST influence on Sahel rainfall

Journal
Climate Dynamics, 43(9-10)

ISSN
0930-7575

Authors
Liu, Y
Chiang, JCH
Chou, C
et al.

Publication Date
2014-11-01

DOI
10.1007/s00382-014-2094-8

Peer reviewed

Atmospheric teleconnection mechanisms of extratropical North Atlantic SST influence on Sahel rainfall

Yuwei Liu
Department of Geography, University of California, Berkeley, California

John C. H. Chiang
Department of Geography and Center for Atmospheric Sciences, University of California, Berkeley, California

Chia Chou
Research Center for Environmental Changes, Academia Sinica, and Department of Atmospheric Sciences, National Taiwan University, Taipei, Taiwan

Christina M. Patricola
Department of Atmospheric Sciences, Texas A&M University, College Station, Texas

Corresponding Author:
Yuwei Liu
Department of Geography, University of California
531 McCone Hall, Berkeley, CA 94720
E-mail: yuwei2341@berkeley.edu
Tel: +15105022181

Abstract

Extratropical North Atlantic cooling has been tied to droughts over the Sahel in both paleoclimate observations and modeling studies. This study, which uses an atmospheric general circulation model (GCM) coupled to a slab ocean model that simulates this connection, explores the hypothesis that the extratropical North Atlantic cooling causes the Sahel droughts via an atmospheric teleconnection mediated by tropospheric cooling. The drying is also produced in a regional climate model simulation of the Sahel when reductions in air temperature (and associated geopotential height and humidity changes) from the GCM simulation are imposed as the lateral boundary conditions. This latter simulation explicitly demonstrates the central role of tropospheric cooling in mediating the atmospheric teleconnection from extratropical North Atlantic cooling.

Diagnostic analyses are applied to the GCM simulation to infer teleconnection mechanisms. An analysis of top of atmosphere radiative flux changes diagnosed with a radiative kernel technique shows that extratropical North Atlantic cooling is augmented by a positive low cloud feedback and advected downstream, cooling Europe and North Africa. The cooling over North Africa is further amplified by a reduced greenhouse effect from decreased atmospheric specific humidity. A moisture budget analysis shows that the direct moisture effect and monsoon weakening, both tied to the ambient cooling and resulting circulation changes, and feedbacks by vertical circulation and evaporation augment the rainfall reduction. Cooling over the Tropical North Atlantic in response to the prescribed extratropical cooling also augments the Sahel drying. Taken together, they suggest a thermodynamic pathway for the teleconnection.

The teleconnection may also be applicable to understanding the North Atlantic influence on Sahel rainfall over the 20th century.

Keywords: *North Atlantic cooling, Sahel, atmospheric teleconnection, monsoon*

1. Introduction

The Sahel region of Africa experienced megadroughts in both the recent and distant past. Drought conditions periodically occurred throughout the late glacial period and the Holocene, each event lasting from decades to several hundred years (Mulitza et al. 2008; Shanahan et al. 2009). More recently, a severe Sahel drought occurred in the late twentieth century, starting as an abrupt reduction in summer rainfall in the 1960's, and lasting for over two decades with limited recovery to date (e.g. Nicholson 1979; Folland et al. 1986). The megadroughts during the later stages of the last glacial period (~50,000 to 14,000 B.P.) have been tied to abrupt cold events over the North Atlantic (Wang et al. 2001; Mulitza et al. 2008; Shanahan et al. 2009; Niedermeyer et al. 2009; Stager et al. 2011). The link between North Atlantic cooling and African droughts persisted during the Holocene, albeit at a weaker level (Shanahan et al. 2009).

Variation in the Atlantic meridional overturning circulation (AMOC) is thought to be the leading cause of the North Atlantic abrupt climate changes. A slowdown of the AMOC reduces the ocean heat transport into the North Atlantic, cooling the extratropical North Atlantic in particular where the mean ocean heat transport convergence occurs. This hypothesis was first proposed by Broecker et al. (1985), and subsequently supported by many other studies (see Alley 2007 for a review). Moreover, simulations of the AMOC slowdown in various coupled climate models (e.g. Vellinga and Wood 2002; Zhang and Delworth 2005; Cheng et al. 2007; Chiang and Friedman 2012) all show global climate impacts including a drying of the Sahel, similar to what is inferred from paleodata (an example can be seen in Figure 5 of Chiang and Friedman 2012). Thus,

there is strong model evidence for a causal link between the North Atlantic cooling and Sahel drought.

Previous studies have led to a hypothesis that atmospheric teleconnections of extratropical North Atlantic cooling cause the impacts in the Sahel seen in AMOC slowdown experiments (see Chiang and Friedman 2012 for a review). Motivation for this hypothesis comes from the fact that an atmospheric general circulation model (AGCM) coupled to a slab ocean, with cooling prescribed in the extratropical North Atlantic (50-70 ℃N) is able to produce very similar global climate changes as in AMOC slowdown experiments. An example simulation using the Community Atmosphere Model 3-slab ocean is shown in Fig. 1. (The simulation is described in detail in Chiang and Friedman 2012.) The simulation shows intense cooling over the extratropical North Atlantic that extends over the whole Northern Hemisphere (NH), in particular to North Africa (Fig. 1a), and a strong rainfall reduction over the Sahel. A significant weakening of the monsoon winds occurs over North Africa as indicated by the anomalous northeasterly wind (Fig. 1b), co-incident with a meridional pressure gradient anomaly between the anomalous high pressure to the north, and low pressure to the south. The model results thus show a continental climate change primarily in temperature and sea level pressure (SLP), which may act to bridge the extratropical North Atlantic cooling to the rainfall reduction over the Sahel.

The mechanism for this atmospheric teleconnection is however still not known; this is the focus of our study. Our approach is centered on the temperature and SLP changes over the Sahara, north of the Sahel, that are apparent in the above simulations. Previous studies support the idea that temperature and (consequently) SLP over North

Africa alters Sahel rainfall. Haarsma et al. (2005) found in observations that Sahel rainfall was related to mean SLP over the Sahara, the latter in turn was related to surface temperatures over North Africa. Biasutti et al. (2009) argued, based on lead–lag correlation, that variation in the Sahara SLP caused variation in the Sahel rainfall. A cursory examination of climate changes associated with Sahara temperature supports this association: the left column of Fig. 2 shows the difference of precipitation, surface temperature and SLP over the North Atlantic and North Africa for July to September between the eight coldest and eight warmest periods in the Sahara since 1979. It shows that a colder Sahara is accompanied by higher Sahara SLP and reduced Sahel rainfall (and increased rainfall along the Guinea Coast). The cooling over the Sahara may weaken the land-sea contrast and thus the monsoon flow. In addition, advection of air with low moist static energy (MSE) limits the northward extent of the land convection zone by displacing high MSE air that favors deep convection, a process known as the "ventilation" mechanism (Chou et al. 2001). The intrusion of low MSE resulting from cooling in the north may thus reduce rainfall over the Sahel. Taken together, these results suggest that cooling in North Africa driven by extratropical North Atlantic cooling can reduce the rainfall over the Sahel, possibly by weakening the land-sea thermal contrast and reducing the MSE.

Our study analyzes the AGCM-slab ocean simulation which produces a reduction in Sahel rainfall in response to prescribed extratropical North Atlantic cooling, with the goal of developing a mechanistic view of this teleconnection. We hypothesize that the North Atlantic influence is communicated to the Sahel through cooling air temperatures over North Africa. We show the plausibility of our temperature hypothesis by showing

that the Sahel rainfall in a regional climate model (RCM) simulation is reduced when we impose tropospheric cooling (and related geopotential height and humidity changes) in the lateral boundary conditions of the model over the North African region. We then apply various diagnostic analyses on the AGCM model simulation, including a moisture budget analysis over West Africa. We also analyze radiative feedback and atmospheric energy transport to determine how extratropical North Atlantic cooling is communicated to lower latitudes. Ultimately, our goal is to understand how and why North Atlantic stadials are linked to rainfall change over the Sahel during past climates, and also to see if such mechanisms are applicable to today's climate.

In the next section, we describe the GCM and the RCM experiments and analysis methods. This is followed by an analysis of the general climate response to extratropical cooling in the GCM in Section 3. We then present results from the RCM in Section 4. In section 5, we show how the North African cooling and extratropical North Atlantic cooling are sustained from an energy budget perspective. The moisture budget of the simulated Sahel rainfall response in the GCM is presented in Section 6. The results are summarized and discussed in Section 7.

2. Experiments and methods

a. Experiments

We use the National Center for Atmospheric Research (NCAR) Community Atmosphere Model version 3.5 (CAM3.5) coupled to a fixed-depth slab ocean model, which interacts thermodynamically with the atmosphere, but has no representation of ocean dynamics (Collins et al. 2006; Chen et al. 2010). The atmospheric model is configured with 26

vertical levels, and 64x128 horizontal grids. A monthly-varying 'Q-flux' is derived from surface fluxes extracted from a fixed-SST simulation forced with global SST climatology, and applied to the model slab. All greenhouse gas and aerosol forcings are constant as present day values.

The slab ocean model is required, as the thermodynamic ocean-atmosphere interaction is essential to communicating the extratropical influence to the tropics (Chiang and Bitz 2005). We use the base configuration described above to undertake two sets of simulations. In the first set, we replace the slab ocean in the North Atlantic over the 45°-60° latitude band with climatological monthly-varying SSTs, and run this configuration to equilibrium. In the second set, we also apply fixed SSTs over the same North Atlantic region, but uniformly cool the applied SST by 2K. The applied cooling is less than half of the typical estimates of extratropical North Atlantic SST changes from interstadials to stadials (~4-6K, van Kreveld et al. 2000), but is sufficient to force a significant reduction in Sahel rainfall (see Section 3). Both simulations are run for 60 years, and the climatology of the last 20 years is used for analysis. The difference between the climatologies is used as the response to the extratropical cooling. The GCM anomalies are shown as the July-August-September (JAS) average in the following sections.

To explicitly show that the cooling over Sahara (and related low MSE) can drive a Sahel rainfall decrease, we apply the cooling to the lateral boundary condition in a regional model simulation of the Sahel. The regional model allows us to isolate the impact of atmospheric cooling anomalies from the Sahara on the Sahel, enabling us to directly test the hypothesis that extratropical North Atlantic cooling leads to Sahel rainfall

reduction through cooling the Sahara. We use the NCAR Weather Research and Forecasting Model (WRF; Skamarock et al. 2008) version 3.3. It is a non-hydrostatic model with 28 vertical levels, with the top of the atmosphere set to 50 hPa. The domain chosen for the simulation is from 16.9 °W to 39.9 °E and from 30.7 °S to 29.3 °N, incorporating the whole of Africa and in particular the Sahara.

The choice of horizontal resolution and physics options basically follows that of the WRF simulation of North Africa by Patricola and Cook (2010). The horizontal resolution used is 90 km, and the physics schemes are the Mellor-Yamada-Janjic planetary boundary-layer scheme (Janjic 1994), the Monin-Obukhov Janjic surface-layer scheme (Monin and Obukhov 1954; Janjic 1994; Janjic 1996; Janjic 2002), the Purdue Lin microphysics scheme (Lin et al. 1983), and the RUC land-surface model (Smirnova et al. 1997). Patricola and Cook (2010) showed that WRF with these options is able to simulate a sufficiently accurate climatology over the Sahel. We use the Zhang-McFarlane cumulus scheme (Zhang and Mcfarlane 1995), which differs from Patricola and Cook (2010) but is the same convection scheme used in our CAM3.5 AGCM simulations. We also use newer radiation schemes that are available in WRF version 3, the RRTMG longwave and shortwave scheme (Mlawer et al. 1997). The simulation time step is 180 seconds.

The National Centers for Environmental Prediction (NCEP) –Department of Energy (DOE) Atmospheric Model Intercomparison Project (AMIP-II) reanalysis (R-2) 6-hourly data (Kanamitsu et al. 2002) are used to specify the lateral boundary conditions for the control simulation. Monthly temperature, geopotential height, and relative humidity anomalies from the GCM runs are then added to the 6-hour reanalysis data for

the cooling simulation. The anomalies are added only at the northern boundary (and the relaxation zone) of the domain, since the purpose of the WRF simulation is to test our hypothesis that it is through modifying atmospheric temperature/energy over the Sahara that extratropical North Atlantic influences Sahel rainfall. Climatological skin temperature in the reanalysis data is used for SST. SST changes are not the focus of our study; and since the land makes up most of the domain, SST has little influence in our simulations. For both the control and cooling simulations, we conduct an ensemble of 10 runs, starting from June 2 of each year from 2000 to 2009 and ending on September 2 of the following year. We run each simulation for fifteen months in order for the soil moisture to spin up, as soil moisture spin-up is important in the semi-arid Sahel region. The daily data from July and August of the following year are averaged as the summer climate. We averaged the ten summer climates separately for the control and cooling runs, and examined their differences.

b. Diagnosis

Two sets of diagnostic analyses are applied to the GCM simulation. In order to understand the communication of the cooling from the extratropical North Atlantic to other regions, we diagnose the atmospheric energy budget by examining both the top of atmosphere (TOA) energy flux and the atmospheric energy transport. We utilize a radiative kernel technique to separate changes of the TOA energy budget due to individual component changes (Soden et al. 2008):

$$\delta R \approx \sum_i \frac{\partial R}{\partial X_i} \delta X_i, \qquad (1)$$

where δR is the change in TOA energy flux, and terms inside the summation designate the change of R due to individual component X_i, including surface temperature T_s,

atmospheric temperature T, water vapor q, surface albedo α, and clouds C. The differential $\partial R/\partial X_i$, which represents the change in TOA energy flux due to a unit change in each component, is the radiative kernel. Kernels for q and C are further split into shortwave (SW) and longwave (LW). We use radiative kernels calculated in CAM3 (Shell et al. 2008; Soden et al. 2008) for all components but clouds. TOA energy flux change due to clouds is calculated as the adjusted cloud radiative forcing (CRF), defined as the difference between the TOA all-sky and clear-sky fluxes, with changes of CRF caused solely by non-cloud components removed (Shell et al. 2008). We also calculate the horizontal advection of MSE to examine how circulations adjust to balance the prescribed cooling and TOA radiative flux changes.

In order to understand the Sahel rainfall response to extratropical cooling, we diagnose the vertically integrated moisture budget equation as in Chou and Neelin (2004) and Chou et al. (2009) but with some modification:

$$\delta P \approx -\langle \omega \frac{\partial \delta q}{\partial p} \rangle - \langle \mathbf{v} \cdot \boldsymbol{\nabla} \delta q \rangle - \langle \delta \omega \frac{\partial q}{\partial p} \rangle + \langle \delta \mathbf{v} \cdot \boldsymbol{\nabla} q \rangle + \delta E, \qquad (2)$$

where $\langle . \rangle$ denotes vertical mass integration through the troposphere, and P, ω, q, p, E and $\mathbf{v}$ denote precipitation, pressure velocity, specific humidity, pressure, evaporation, and horizontal velocity, respectively. The total rainfall change, δP, thus can be approximated by the summation of 1) anomalous vertical moisture transport associated with anomalous moisture δq, 2) anomalous horizontal moisture transport associated with anomalous moisture δq, 3) anomalous vertical moisture transport associated with anomalous vertical flow $\delta \omega$, 4) anomalous horizontal moisture transport associated with anomalous horizontal flow $\delta \mathbf{v}$ and 5) anomalous evaporation, as shown from left to right respectively in the right hand side (RHS) of the equation above.

3. Climate response to extratropical North Atlantic cooling

a. Climate response over the Atlantic and North Africa

Surface temperature and SLP are closely related to the Sahel rainfall in both observations and model simulations (Haarsma et al. 2005; Biasutti et al. 2009; Liu and Chiang 2012); therefore we begin presenting the GCM-simulated JAS averaged climate response to extratropical North Atlantic cooling by showing those three fields (right column of Fig. 2). In the control run, the oceanic ITCZ is located north of the equator over the Atlantic, extending into northeast Brazil and the west coast of the Sahel. Prescribed extratropical North Atlantic cooling in turn leads to a cooling of the North Tropical Atlantic SST and a southward displacement of the Atlantic ITCZ; these responses are well-known (e.g. Chiang and Bitz 2005). Precipitation in the Sahel is reduced by over 25% in response to the cooling, with a maximum anomaly of over 1 mm/day (Fig. 2d). Temperatures to the north and west of the Sahel are colder, with a ~1K surface cooling across the midlatitude Atlantic and Europe (Fig. 2e). The cooling south of 40 ºN, though smaller, extends all the way to near the equator over the ocean, and to the boundary between the Sahara and the Sahel over North Africa. The maximum cooling over the Sahara is more than 0.5 K, and located near the simulated heat low around 20 ºN. Over the Sahel, temperatures are warmer in association with reduced rainfall, which supports a reduced evaporative cooling and increased solar radiation at the surface.

SLP over the Sahara is also increased in association with the North Atlantic cooling (Fig. 2f); this response is likely causally linked to the cooling (discussed later). The pressure increase over North Africa peaks near the climatological Sahara Low with a magnitude of ~1 hPa, leading to decreased meridional SLP contrast between the Sahara

and the Gulf of Guinea. Overall, a broad cooling and coincident SLP increase appear over the Atlantic and North Africa, and rainfall is reduced over the Sahel with a slight increase over the Guinean Coast, consistent with results from previous studies on extratropical North Atlantic cooling (e.g. Mulitza et al. 2008; Liu and Chiang 2012). The simulated response in North African climate to extratropical North Atlantic cooling resembles the observed difference of climate in cold and warm Sahara periods (left column of Fig. 2), lending confidence to our hypothesis that temperature over the Sahara broadcasts the extratropical signal to the Sahel.

Extratropical North Atlantic SST cooling induces changes in atmospheric temperature, specific humidity, and clouds, which exert feedbacks to the initial temperature change by altering the TOA energy budget. We present these changes of in Fig. 3. Mean tropospheric temperature, defined as the mass-weighted vertical average of atmospheric temperature from the surface to 100mb, broadly decreases in the domain (Fig. 3a). Mean tropospheric specific humidity, calculated similarly to mean tropospheric temperature, decreases in response to the cooling (Fig. 3b), following the Clausius–Clapeyron relation in regions where relative humidity varies little, especially north of the Sahel. The drop in humidity appears to peak over convective regions, in particular in the Sahel where mean tropospheric humidity is reduced by about 0.3 g/kg; this is consistent with the reduction in convection there. Changes in both mean tropospheric temperature and humidity (and also geopotential height which is small, not shown) result in a substantial decrease in MSE (Fig. 3c), with two maxima corresponding to the maximum change of temperature in the extratropics, and of humidity in the Sahel.

In the extratropics, cooler SST over the North Atlantic favors boundary layer inversions, leading to an increase in low clouds (surface to 700 mb, Fig. 3d). In the tropics, low clouds decrease over the Sahel in association with the reduction in convection. High clouds (400mb to the model top) decrease over both the northern ocean and the Sahel and increase over the southern edge of climatological ITCZ and northeast Brazil, in accordance with the rainfall change (Fig. 3e). The change in middle clouds (700 mb to 400 mb) generally follows that of low clouds except for a slight decrease over the extratropical North Atlantic (not shown).

b. Vertical profile of climate anomalies over North Africa

The GCM-simulated Sahelian rainfall reduction in response to extratropical North Atlantic cooling largely results from anomalous convection and monsoonal flow. We present vertical profiles of the circulation, temperature and humidity anomalies from the cooling minus control GCM simulations to illustrate this point (Fig. 4). All fields are averaged between 10 °W and 30 °E. Substantial cooling reaches 20 °N, with a maximum of more than 0.7K in the middle troposphere (Fig. 4a). The strong cooling over the Sahara results in a meridional temperature gradient anomaly. Over the Sahel between 10 °N and 20 °N, a vertical dipole is seen with warming near the surface and cooling in the middle and upper troposphere. The dipole is likely a consequence of the increase in the Bowen ratio at the surface and the suppression of deep convection; combined, they lead to less water vapor being evaporated into the atmosphere from the surface and brought to the middle troposphere for condensation, while more heat warms the lower troposphere in the form of sensible heat. The specific humidity is reduced considerably over North Africa and the reduction is largely confined to the lower troposphere, consistent with the

reduction of convection there (Fig. 4b). The magnitude of change generally reaches 0.3 g/kg, and can exceed 0.5 g/kg in the lower troposphere over the Sahel.

The vertical wind anomaly shows a 20% increase in subsidence north of the Sahel and a decrease in ascent over the Sahel (Fig. 4c). The substantial sinking anomaly near the climatological subsidence zone over the Sahara acts to balance the cooling through adiabatic compression. Over the Sahel, there is a dipole with enhanced (weakened) uplift below (above) 800mb, indicating decreased deep convection and a slight enhancement of shallow thermal convection.

The upper level tropical easterly jet (TEJ) at 200mb, with a climatological core around 10 ºN, induces upper level divergence and thus lower level convergence and convection (Nicholson 2009). In the experiment, the TEJ is weakened in response to the negative temperature gradient (Fig. 4d), similar to the observed circulation change in Sahel dry years as found by Nicholson (2009).

The mid-level African easterly jet (AEJ) is only vaguely simulated at 600mb around 17 ºN in the control run. A strong easterly anomaly, however, appears at 12 ºN between 500mb and 800mb in the experiment, suggesting a southward shift and strengthening of the AEJ. The easterly anomaly is likely caused by the positive temperature gradient as a result of the low-level warming between 10 ºN and 20 ºN (Fig. 4a). Grist and Nicholson (2001) found in observations that the AEJ induces cyclonic (anticyclonic) shear to its south (north) and that a southward AEJ shift likely displaces the rainbelt southward, thus reducing the rainfall over the Sahel. Cook (1999) and Patricola and Cook (2008) found that changes in the AEJ, which depend on the meridional temperature/soil moisture gradients, can also reduce rainfall by transporting

moisture away from the Sahel. Therefore, a positive feedback exists in our simulation: as a rainfall decrease reduces soil moisture and thus leads to surface warming, a consequent positive temperature gradient in the low level strengthens the AEJ and displaces it southward, which in turn further reduces rainfall over the Sahel.

The southwesterly monsoon flow, which extends to 800mb climatologically, is weakened by up to 30% in the lower troposphere (Fig. 4d and 4e), probably due to the diminished meridional temperature/pressure gradient. Climatological northerlies from the Sahara converge with the monsoon flow over the Sahel. The strengthened northerlies in the cooling simulation bring anomalously dry and cool air to the Sahel, weakening the low-level convergence and shifting it southward.

4. Testing the temperature hypothesis using a WRF simulation of the Sahel

While the GCM-modeled Sahel climate response is consistent with the influence of atmospheric and surface cooling over the Sahara, it does not demonstrate causality. We explicitly show that the cooling can drive a rainfall decrease over the Sahel, by applying temperature, humidity, and geopotential height anomalies as exterior boundary condition in a WRF simulation of the Sahel. With those GCM anomalies applied only to the northern boundary of the RCM domain, the WRF simulation produces a response in Sahel climate to Sahara tropospheric cooling comparable to the response in Sahel climate to extratropical North Atlantic cooling in the GCM. The simulated precipitation anomaly (Fig. 5a) exhibits finer structures due to the higher resolution of the WRF model, but the overall change resembles that in the GCM. Drying with a maximum of over 1 mm/day

appears between 10 ºN and 20 ºN over North Africa; both the location and magnitude of this drying are comparable to the GCM response (Fig. 2d). Scattered drying and wetting are shown south of the Sahel in WRF, leading to a neutral or slightly positive overall precipitation change as in the GCM. The overall precipitation change, in particular the substantial decrease in the Sahel, suggests a retreat of the monsoon convection, consistent with the ventilation mechanism where low MSE from the north limits the extent of land convection. Precipitation north of 10 ºN along the west coast, which is influenced by the oceanic ITCZ (Fig. 2d), exhibits little change, as change in SST is not taken into account in the WRF simulation.

The regional model also reproduces the surface temperature and pressure response to atmospheric cooling (Fig. 5b and 5c) with magnitudes comparable to those in the GCM experiment. Cooling spreads from the northern boundary of the domain to the vicinity of Sahel, where the surface warms as a result of the rainfall reduction. As WRF does not output SLP, we take surface pressure instead for comparison. The surface pressure in WRF (Fig. 5c), similar to the SLP in the GCM (Fig. 2f), increases over the Sahara, reducing the strength of the Sahara Low and thus the pressure gradient between North Africa and the tropical Atlantic.

Vertical profiles of the WRF-simulated wind anomalies, averaged from 10 ºW to 30 ºE are shown in Fig. 5 (compare to the GCM fields in figure 4). The WRF responses to prescribed anomalies relevant to cooling on the northern lateral boundary condition are largely comparable to those of the GCM simulation, except that since the mean Sahel uplift region is located somewhat north (~20 ºN) of the GCM uplift region (~17 ºN), the WRF anomalies are similarly shifted. The sinking anomaly north of 20 ºN and the vertical

dipole over the Sahel are apparent in WRF simulation (Fig. 5d), although the near-surface uplift anomaly south of 20 ºN looks deeper in WRF than in the GCM. The response of the zonal wind (Fig. 5e) in the upper troposphere, which basically follows the thermal wind, is identical with that in CAM (Fig. 4d). However, unlike the anomalous low-level northerlies south of 30 ºN in the GCM, WRF exhibits anomalous low-level northerlies from 15 ºN-30 ºN, and anomalous low-level southerlies to the south of 15 ºN (compare Fig. 5f and 4e). As a consequence, there is a slight southward shift of the low-level convergence center toward the Guinea Coast, bringing about the anomalous low-level convergence around 18 ºN and compensating divergence around the 600mb level. The shifted convergence is weaker and the convection is shallower in the cooling simulation compared with the climatology, consistent with the reduction in rainfall.

Differences in details aside, anomalies relevant to cooling from CAM3.5 forced only at the northern lateral boundary of the WRF domain generally simulate the Sahel rainfall reduction and associated temperature, pressure, and circulation changes as in the GCM experiment which is forced with extratropical North Atlantic SST cooling. Our WRF simulation thus provides strong evidence that the Sahel rainfall changes in the GCM experiment result from large-scale cooling in tropospheric temperatures north of the Sahel.

5. How is the cooling communicated and maintained?

Cooling over the Sahara is key to our proposed teleconnection. It then begs the question of how the temperature changes are communicated from the high-latitude North Atlantic. We have shown that the prescribed 2K SST cooling in the extratropical North Atlantic causes significant cooling in the Atlantic sector, with a magnitude generally larger than

1K in the midlatitude Atlantic and Europe, and as much as 0.5K near the Sahel. How is such a strong cooling response maintained both near and far from the source?

We first explore this question by evaluating the radiative feedbacks that help amplify and maintain the cooling far from its source region. TOA radiative flux anomalies in response to the North Atlantic cooling in the GCM simulations are shown in Fig. 6, separated into contributions by cloud, moisture, and temperature changes (downward is positive, so negative values mean energy loss and thus more cooling of the atmosphere, acting as a positive feedback). As shown in Fig. 3, a sizable increase of low clouds, presumably stratus, appears over the ocean in association with prescribed cooling; this is likely due to the surface-cooling induced boundary layer inversion. The stratus cloud cover exerts a strong positive feedback by reflecting more SW than it absorbs LW (Fig. 6a and 6c). This cooling effect dominates in the extratropics. On the other hand, cloud cover decreases over North Africa, in particular over the Sahel, consistent with the reduced convection there. Reduced cloud cover allows for more incoming SW to the atmosphere but also leads to more outgoing longwave radiation (OLR) (Fig. 6a and 6c). The two competing effects largely cancel, leaving a slight SW gain over the Sahel, which partially contributes to the surface warming. Overall, cloud feedbacks are positive and dominant in extratropics, but relatively weak in tropics (Fig. 6e).

A negative LW flux anomaly due to reduced tropospheric humidity appears across the North Atlantic and into Europe and North Africa (Fig. 6b), leading to a considerable increase in clear-sky OLR, a major positive radiative feedback in tropics. Water vapor is also a SW absorber and thus contributes to a small positive feedback to cooling from reducing shortwave absorption (not shown). Maximum cooling from the LW moisture

391 feedback is collocated over the Sahel with the maximum of water vapor reduction.
392 Another positive feedback involves the surface albedo change (not shown), as the
393 brighter surface reflects SW as more ice forms in high latitudes. Decreased incoming SW
394 due to albedo is also found over the Sahel, with a smaller magnitude than that in high
395 latitudes.

396 Taken together, total clouds, moisture, and surface albedo yield an overall
397 positive feedback in the Atlantic sector, as well as over North Africa (Fig. 6f). In
398 particular, the positive SW cloud feedback dominates in the extratropics whereas the
399 positive LW moisture feedback prevails in the tropics. All the positive feedbacks lead to
400 further energy loss in addition to the prescribed cooling, and such energy loss requires a
401 decrease in surface and tropospheric temperature and change in lapse rate to compensate
402 by reducing OLR (Fig. 6d).

403 To better quantify the significance of the cloud and water vapor feedback on
404 enhancing atmospheric cooling, we estimate the atmospheric temperature anomalies
405 associated with those feedbacks. We start with the vertically integrated energy budget,
406 which, in equilibrium, is

407 $$0 = \delta F_A + \delta F_s + \delta R\ , \qquad (3)$$

408 where δF_A is anomalous horizontal heat convergence, δF_s is anomalous surface flux into
409 the atmosphere (which is nonzero over the extratropical North Atlantic in our
410 simulation), and δR is the change in TOA energy flux. Expanding δR as in equation (1),
411 and rearranging the above equation give

412 $$\delta T = -\frac{1}{\frac{\partial R}{\partial T}}(\delta R_c + \delta R_{wlw} + \delta R_{rest} + \delta F_A + \delta F_s). \quad (4)$$

The first three terms in the parentheses on the RHS are the TOA energy flux anomalies related to total cloud feedback, δR_c, LW water vapor feedback, δR_{wlw}, and all other feedbacks, δR_{rest}, respectively. Each energy flux anomaly in the parentheses is divided by the vertical integral of the air temperature kernel, $\partial R/\partial T$, to yield the partial temperature change of a "slab" atmosphere due to the anomaly. We present the first two terms on the RHS of equation (4), partial temperature changes due to clouds and water vapor, in Fig. 6g and 6h. As the spatial variance of the temperature kernel is small (not shown), the spatial pattern of the feedback-derived air temperature change generally follows the TOA flux anomalies, but the magnitude is three times as large as the simulated mean tropospheric temperature anomaly (Fig. 3a). The temperature decrease due to cloud feedbacks is over 2K in most of the extratropical North Atlantic, with a maximum of over 4K; whereas the maximum modeled mean tropospheric temperature cooling is ~1K; the water vapor feedback dominates in the tropics, in particular over North Africa, and the consequent partial temperature change is slightly larger than that in the simulation.

We now examine how the energy transport by the atmopheric circulation adjusts to balance the TOA radiative flux changes. We calculate the change in the horizontal advection of MSE (Fig. 7a), decomposed into contributions by anomalous MSE advection by the climatological flow (Fig. 7b), and advection of climatological MSE by the anomalous flow (Fig. 7c). The residual, mainly consisting of the non-linear term, is small and thus neglected. Overall, horizontal MSE advection propagates cooling from the extratropical North Atlantic downstream - to Europe, the subtropical North Atlantic, and North Africa (Fig. 7a). The magnitude much larger than that of the radiative feedbacks.

436 The low MSE advection is completed mainly by the climatological westerlies in the
437 extratropics (Fig. 7b), and by anomalous northely flow over North Africa (Fig. 7c). The
438 advection further decomposed into contributions from each component of MSE, reveals
439 that over the Sahara the cooling is induced by cold air invasion, while in the Sahel it is
440 caused by decreased latent heat energy input from weakened monsoon flow (not shown).
441 Intrusion of air with low moist static energy (MSE) to the subtropics limits the
442 poleward extent of the continental convergence zone by displacing high MSE air that
443 favors deep convection, a mechanism known as ventilation (Chou *et al.* 2001). If the
444 advection of low MSE air into North Africa is indeed the mechanism for the Sahel
445 rainfall reduction, can the Tropical North Atlantic – which also cools in response to
446 imposed extratropical North Atlantic cooling – act to augment drying over the Sahel? In
447 order to test this, we perform two idealized simulations: in the first, we apply
448 extratropical North Atlantic cooling but keep the Tropical North Atlantic SST fixed to the
449 climatology (by replacing the slab ocean there with prescribed SST); in the second, we
450 prescribe SST cooling only over the Tropical North Atlantic at the same level as in the
451 'usual' slab-ocean simulation with extratropical North Atlantic cooling. Thus, the first
452 simulation tests the teleconnection without the Tropical North Atlantic SST feedback,
453 and the second is the feedback contribution. The results (figures not shown) show that the
454 Tropical North Atlantic SST feedback does indeed augment the Sahel drying, but the
455 majority (over two thirds) of the drying is achieved without this feedback. This result is
456 consistent with the ventilation argument, as the westerlies are stronger in the midlatitudes
457 whereas in the tropics the climatological flow is easterly.

458 In summary, radiative feedbacks, tropical SST feedbacks, and atmospheric
459 transport cooperate to communicate extratropical cooling to the Sahel. Extratropical
460 North Atlantic cooling - augmented by a positive low cloud feedback - is advected
461 downstream by the climatological midlatitude westerlies, cooling Europe and North
462 Africa. Circulation changes over North Africa further reduce the MSE, by importing cold
463 air and countering the advection of latent heat energy from the monsoon flow. Cooling
464 over North Africa is further amplified by a reduced greenhouse effect from decreased
465 atmsopheric specific humidity. Finally, a cooler Tropical North Atlantic also acts to
466 augment drying over the Sahel.

467 6. Moisture budget analysis of the Sahel rainfall response

468 Our results thus far point strongly to cooling north of the Sahel as the cause of the Sahel
469 rainfall change. In this section we diagnose the moisture budget over the Sahel in the
470 GCM simulation, to infer how the rainfall changes are linked to the cooling.

471 *a. Moisture budget analysis*

472 Fig. 8 shows each term of the vertically-integrated moisture budget from the RHS of
473 equation (2) (note these terms, factoring in the latent heat of vaporization, are plotted in
474 energy units, W m^{-2}). Changes in specific humidity contribute considerably to the
475 reduction of rainfall over the Sahel (Fig. 8a and 8b), and its effect is mainly through
476 vertical transport anomalies. Humidity decreases primarily in the lower troposphere,
477 resulting in a negative vertical moisture gradient anomaly (Fig. 4b). Therefore over the
478 Sahel (a region of mean ascending motion) this term leads to drying (Fig. 8a). The
479 reverse effect - that a weakened vertical humidity gradient makes the downward transport

less arid - holds for subsidence regions of the Sahara. The humidity exhibits a positive meridional gradient anomaly over North Africa, as the Sahel dries out more than the Sahara **(**Fig. 3b**)**. With the climatological wind being northerly at the boundary between the Sahara and Sahel, the humidity anomaly wets the transition zone (Fig. 8b).

The term of the largest magnitude on the RHS of equation (2) is the anomalous vertical moisture transport caused by the sinking anomaly (Fig. 8c). The dipole at the very western edge of the Sahel with a negative anomaly in the north and positive anomaly in the south marks the southward shift of the Atlantic marine ITCZ. Further inland, such a dipole-like signature is only seen in Central and East Africa, with the rest of the area being dominated by near-uniform drying.

Reduced horizontal moisture transport by changes in the horizontal winds contributes significantly to the local rainfall reduction over central Sahel (Fig. 8d). This is mainly due to a reduction of the southerly flow, as demonstrated in a further split of this term into contributions from zonal and meridional wind (not shown). Evaporation decreases between 15 ºN and 20 ºN (Fig. 8e), primarily in association with the reduced soil moisture; warmer temperatures here would tend to increase evaporation, but evaporation over the Sahel semi-arid region is moisture- rather than temperature-limited. This is in contrast to West Africa along 10 ºN, where surface warming actually increases evaporation.

b. Processes of the Sahel rainfall reduction

Three major processes of the Sahel rainfall reduction are suggested from the above analysis. The first is the “direct moisture effect”, the change in vertical moisture transport due to anomalous specific humidity. This effect has been proposed previously by Chou

503 and Neelin (2004) to explain the tropical precipitation response to global warming; they
504 demonstrated that an increase in gross moisture stratification due to low-level moisture
505 increases with global warming leads to increased rainfall in climatological convergence
506 regions, as part of the rich-get-richer mechanism. In our cooling simulation, the direct
507 moisture effect acts in the opposite way by decreasing rainfall in convective regions, or
508 rich-get-poor (Fig. 8a). The decrease in specific humidity comes about partly due to the
509 tropospheric cooling in vicinity of the Sahel that makes the atmosphere hold less
510 moisture, and partly as a result of circulation changes.

511 The second process, the change in the vertical moisture transport due to
512 anomalous vertical wind, also contributes significantly to Sahel rainfall reduction. This
513 term is a dynamic feedback associated with a reduction of low-level moisture content
514 (Chou and Neeling 2004). An analysis of the local MSE budget (not shown) following
515 Chou and Neelin (2004) reveals both an increase of moist stability due to drying and an
516 increase of dry instability due to low-level warming. The former overtakes the latter,
517 resulting to a more stable atmosphere, consistent with the weakened convection.

518 The third process is related to the monsoon flow. Cooling over the Sahara reduces
519 the land-sea contrast in the West African monsoon regime, leading to a positive pressure
520 anomaly in the Sahara and a weakening of the meridional pressure gradient (Fig. 2f). The
521 southwesterly monsoon flow carrying moisture inland from the Gulf of Guinea is reduced
522 accordingly, while dry air advection from the Sahara to the Sahel increases (Fig 4e);
523 these lead to the moisture transport changes due to anomalous horizontal wind seen in
524 Fig. 8d.

In addition to the three main processes, reduced evaporation over the Sahel plays a significant role in reducing rainfall. This presumably arises from a soil-moisture feedback – a positive feedback loop is set up once decreased precipitation reduces soil moisture, which in turn weakens evaporation and thus lower-tropospheric moisture available for precipitation. The evaporation effect is more restricted to the northern part of the rainfall reduction, presumably because soil moisture is a greater limiting factor for precipitation close to the Sahel-Sahara transition. On the other hand, toward the Guinea Coast the increased evaporation tends to enhance rainfall.

Taken together, the Sahel rainfall reduction is associated with reduced specific humidity, reduced vertical flow and weaker monsoon flow, and reduced local evaporation. Those changes are consistent with the decreased land-sea contrast created by the cooling and consequent circulation change, and dynamic/thermodynamic feedbacks of the two. However, given that the moisture budget is a diagnostic analysis, no causal relationship should be drawn from the results before further mechanistic study is done.

7. Concluding notes

a. Conclusion

We investigate teleconnection mechanisms of how extratropical North Atlantic cooling reduces summertime rainfall over the Sahel, using simulations of atmospheric general circulation model (the NCAR Community Atmosphere Model version 3.5, CAM3.5) coupled with a slab ocean. The hypothesis we propose is that the extratropical North Atlantic influence is communicated to the Sahel through air temperatures over North Africa, and that the Sahel rainfall is a direct response to the temperatures. Forced by 2K

cooling in extratropical North Atlantic SST, the AGCM simulates surface cooling which spreads throughout the North Atlantic and surrounding continents, and penetrates into the Sahara (Fig. 2e). Rainfall decreased by more than 25% in the semi-arid Sahel area between 10 ºN and 20 ºN across Africa (Fig. 2d). Other climate signatures are linked to the cooling, including a low cloud cover increase in the extratropics (Fig. 3d), SLP increase (Fig. 2f) and humidity and MSE decrease (Fig. 3b and 3c) north of the Sahel, enhanced subsidence over the Sahara, and weakened upper level easterly jet and low level monsoon flow over the Sahel (Fig. 4).

We then use a regional model – the Weather Research and Forecasting (WRF) model – to explicitly show that cold air anomalies over the Sahara can drive rainfall decreases over the Sahel. We apply cooling and related decreased geopotential height and humidity forcings derived from the GCM simulation as the northern lateral boundary condition in the WRF model, whose domain is set over Africa; the resulting changes to the Sahel rainfall and North African climate were broadly similar to the GCM response (Fig. 5). Our WRF simulation thus strongly bolsters our hypothesis that the Sahel rainfall changes in the GCM forced with extratropical North Atlantic cooling result from large-scale cooling to the tropospheric temperatures north of the Sahel.

Our analysis suggests that the teleconnection is mediated by the advection of anomalously cold, dry air from the extratropical North Atlantic to North Africa (Fig. 7). Climatological midlatitude westerlies bring low MSE air from the extratropics to North Africa, where the MSE is further reduced by increased (decreased) import of cold (wet) air by anomalous northerlies. This ventilation effect removes heat from land and thus hinders convection, as shown in Chou et al. (2001). We also find that the Tropical North

570 Atlantic, which also cools in response to the extratropical North Atlantic cooling,
571 augments the Sahel drying; but this feedback response is relatively small.

572 We find that radiative feedbacks also augment the teleconnection. A radiative
573 kernel (Shell et al. 2008; Soden et al. 2008) analysis on our simulation show that the
574 positive cloud shortwave feedback considerably enhances the cooling in the extratropics,
575 in particular over the North Atlantic, while positive moisture longwave feedbacks
576 dominates in the tropics (Fig. 6). It suggests that these feedbacks are able to leverage the
577 effects of extratropical North Atlantic cooling: specifically, increased low clouds form
578 over the extratropical North Atlantic in response to the imposed surface cooling could
579 have led to over a 2K uniform drop in atmospheric temperature, if no negative feedback
580 or horizontal heat convergence were present (Fig. 6g); Decreases in tropospheric specific
581 humidity reduce the associated greenhouse effect – this cooling is specifically effective in
582 acting remotely from the North Atlantic (Fig. 6h).

583 Finally, we analyze the vertically-integrated moisture budget over the Sahel,
584 following Chou and Neelin (2004) and Chou et al. (2009), to explore the link between the
585 contiguous cooling and the Sahel rainfall response. The decreased Sahel rainfall was
586 primarily balanced by the direct moisture effect, stability increase, and monsoon
587 weakening, processes that were tied to the ambient cooling and resulting circulation
588 changes (Fig. 8). Positive feedbacks between soil moisture and precipitation also
589 contributed to the rainfall reduction. These analyses explicitly link the rainfall reduction
590 to the cooling, but do not assign causality.

591 Our analysis demonstrates the plausibility of the atmosphere-mediated mechanism
592 for the propagation of cooling, and the key factors in maintaining the teleconnection once

593 it is set up. However, more work is required to develop and test the teleconnection
594 mechanism. An examination of the evolution of transient radiative feedbacks,
595 atmospheric circulation and related energy transport, and the interaction of the two after
596 the onset of the extratropical North Atlantic cooling, would be useful in this regard.

597 ***b. Relevance to the 20th century Sahel Drought***

598 The proposed teleconnection mechanism may be relevant to the recent Sahel
599 drought that occurred in the late 1960's (e.g. Nicholson 1979; Folland et al. 1986).
600 Various sources including greenhouse gases, anthropogenic aerosols, SSTs, and local
601 land changes are linked to the Sahel drought (e.g. Folland et al. 1986; Folland et al. 1991;
602 Xue and Jagadish 1993; Rowell et al. 1995; Fontaine et al. 1998; Rotstayn and Lohmann
603 2002; Bader and Latif 2003; Giannini et al. 2003; Biasutti and Giannini 2006; Held et al.
604 2006; Hoerling et al. 2006; Zhou et al. 2008; Kawase et al. 2010; Liu and Chiang 2012),
605 among which SSTs, in particular over the Atlantic, have been shown to play a key role.
606 Folland et al. (1986) showed that the onset of the Sahel drought was tied to an
607 interhemispheric SST gradient with cooling in the Northern Hemisphere and warming in
608 the Southern Hemisphere, particularly in the Atlantic. Apart from the gradient, a striking
609 feature related to the drought is intense cooling in high-latitude North Atlantic. The effect
610 of this SST pattern in drying the Sahel has been confirmed in subsequent studies (Folland
611 et al. 1991; Rowell et al. 1995; Fontaine et al. 1998). Liu and Chiang (2012) specifically
612 showed that the Sahel drought is tied to cooling over Eurasia and North Africa, and both
613 the drought and cooling are a consistent climate signature with the observed extratropical
614 North Atlantic SST drop in the late 1960's. This linkage suggests that the paleo-scenario
615 that extratropical North Atlantic cooling leads to a Sahel rainfall reduction also applies to

616 the twentieth century. The current study may shed light on the mechanism of
617 teleconnection from the North Atlantic to the Sahel in modern climate.
618

619 8. Acknowledgements

620 This research is supported by the National Science Foundation (NSF AGS-1143329 and
621 NSF EAR-0909195). The authors would like to thank Inez Fung, Shih-Yu Lee, Andrew
622 Friedman and Ching-Yee Chang for useful and enlightening discussions. YL thanks
623 Ivana Cvijanovic for helping design the GCM simulation, Alexandra Jonko for assistance
624 with using the radiative kernel technique, Andrew Friedman and Meghan Thurlow for
625 editing the manuscript for grammar and usage. All reanalysis data are provided by the
626 NOAA/OAR/ESRL PSD, Boulder, Colorado, USA, at http://www.esrl.noaa.gov/psd/.

627 9. References

628 Adler RF, Huffman GJ, Chang A, et al. (2003) The version-2 global precipitation
629 climatology project (GPCP) monthly precipitation analysis (1979-present). J
630 Hydrometeorol 4:1147-1167. doi: 10.1175/1525-
631 7541(2003)004<1147:TVGPCP>2.0.CO;2
632 Alley RB (2007) Wally was right: Predictive ability of the North Atlantic "conveyor belt"
633 hypothesis for abrupt climate change. Annu Rev Earth Planet Sci 35:241–272.
634 Bader J, Latif M (2003) The impact of decadal-scale Indian Ocean sea surface
635 temperature anomalies on Sahelian rainfall and the North Atlantic Oscillation.
636 Geophys Res Lett 30:2169.

637 Biasutti, M, Giannini, A. (2006). Robust Sahel drying in response to late 20th century
638 forcings. Geophys Res Lett, 33(11).
639 Biasutti M, Sobel A, Camargo S (2009) The Role of the Sahara Low in Summertime
640 Sahel Rainfall Variability and Change in the CMIP3 Models. J Clim 22:5755–5771.
641 doi: 10.1175/2009JCLI2969.1
642 Broecker WS, Peteet DM, Rind D (1985) Does the ocean-atmosphere system have more
643 than one stable mode of operation? Nature 315:21–26. doi: 10.1038/315021a0
644 Chen, H, Zhou T, Neale R, Wu X, Zhang G (2010) Performance of the new NCAR
645 CAM3. 5 in East Asian summer monsoon simulations: Sensitivity to modifications of
646 the convection scheme. J Clim, 23:3657–3675.
647 Cheng W, Bitz CM, Chiang JCH (2007) Adjustment of the global climate to an abrupt
648 slowdown of the Atlantic meridional overturning circulation. Geophys Monogr,
649 173:295.
650 Chiang JCH, Bitz CM (2005) Influence of high latitude ice cover on the marine
651 Intertropical Convergence Zone. Clim Dyn 25:477–496.
652 Chiang JCH, Friedman AR (2012) Extratropical Cooling, Interhemispheric Thermal
653 Gradients, and Tropical Climate Change. Annu Rev Earth Planet Sci Vol 40 40:383–
654 412.
655 Chou C, Neelin J, Su H (2001) Ocean-atmosphere-land feedbacks in an idealized
656 monsoon. Q J R Meteorol Soc 127:1869–1891. doi: 10.1002/qj.49712757602
657 Chou C, Neelin JD (2004) Mechanisms of global warming impacts on regional tropical
658 precipitation. J Clim 17:2688–2701. doi: 10.1175/1520-
659 0442(2004)017<2688:MOGWIO>2.0.CO;2

660 Chou C, Neelin JD, Chen C-A, Tu J-Y (2009) Evaluating the "Rich-Get-Richer''
661 Mechanism in Tropical Precipitation Change under Global Warming. J Clim
662 22:1982–2005. doi: 10.1175/2008JCLI2471.1
663 Collins W, Rasch P, Boville B, et al. (2006) The formulation and atmospheric simulation
664 of the Community Atmosphere Model version 3 (CAM3). J Clim 19:2144–2161.
665 Cook K (1999) Generation of the African easterly jet and its role in determining West
666 African precipitation RID B-4998-2011. J Clim 12:1165–1184. doi: 10.1175/1520-
667 0442(1999)012<1165:GOTAEJ>2.0.CO;2
668 Folland CK, Owen J, Ward MN, Colman A (1991) Prediction of seasonal rainfall in the
669 sahel region using empirical and dynamic methods. J Forecast 10:21–56. doi:
670 10.1002/for.3980100104
671 Folland CK, Palmer TN, Parker DE (1986) Sahel Rainfall and Worldwide Sea
672 Temperatures, 1901-85. Nature 320:602–607.
673 Fontaine B, Trzaska S, Janicot S (1998) Evolution of the relationship between near global
674 and Atlantic SST modes and the rainy season in west Africa: statistical analyses and
675 sensitivity experiments. Clim Dyn 14:353–368. doi: 10.1007/s003820050228
676 Giannini A, Saravanan R, Chang P (2003) Oceanic forcing of Sahel rainfall on
677 interannual to interdecadal time scales. Science 302:1027–1030.
678 Grist J., Nicholson S. (2001). A study of the dynamic factors influencing the rainfall
679 variability in the West African Sahel. J Clim., 14(7), pp.1337-1359
680 Haarsma RJ, Selten FM, Weber SL, Kliphuis M (2005) Sahel rainfall variability and
681 response to greenhouse warming. . Geophys Res Lett 32: L17702.

682 Held IM, Delworth TL, Lu J, et al. (2006) Simulation of Sahel drought in the 20th and
683 21st centuries. Natl. Acad. Sci. U. S. A, 103(4), pp.1152–1153.
684 Hoerling M, Hurrell J, Eischeid J, Phillips A (2006). Detection and attribution of
685 twentieth-century northern and southern African rainfall change. J Clim, 19(16),
686 pp.3989–4008.
687 Janjic Z (1994) The Step-Mountain Eta Coordinate Model - Further Developments of the
688 Convection, Viscous Sublayer, and Turbulence Closure Schemes. Mon Weather Rev
689 122:927–945. doi: 10.1175/1520-0493(1994)122<0927:TSMECM>2.0.CO;2
690 Janjic Z (1996) The surface layer in the NCEP Eta Model. Eleventh Conference on
691 Numerical Weather Prediction, Norfolk, VA, 19-23 August; Amer Meteor Soc,
692 Boston, MA 354–355.
693 Janjic ZI (2002) Nonsingular implementation of the Mellor–Yamada level 2.5 scheme in
694 the NCEP Meso model. NCEP office note 437:61.
695 Kalnay E, Kanamitsu M, Kistler R, et al. (1996) The NCEP/NCAR 40-year reanalysis
696 project. Bull Amer Meteor Soc 77:437–471.
697 Kanamitsu M, Ebisuzaki W, Woollen J, et al. (2002) NCEP-DOE AMIP-II Reanalysis
698 (R-2). Bull Am Meteorol Soc 83:1631–1644.
699 Kawase H, Abe M, Yamada Y, et al.(2010). Physical mechanism of long-term drying
700 trend over tropical North Africa. Geophys Res Lett, 37, L09706
701 Lin Y, Farley R, Orville H (1983) Bulk Parameterization of the Snow Field in a Cloud
702 Model. Journal of Climate and Applied Meteorology 22:1065–1092. doi:
703 10.1175/1520-0450(1983)022<1065:BPOTSF>2.0.CO;2

704 Liu Y, Chiang JCH (2012) Coordinated Abrupt Weakening of the Eurasian and North
705 African Monsoons in the 1960s and Links to Extratropical North Atlantic Cooling. J
706 Clim 25:3532–3548. doi: 10.1175/JCLI-D-11-00219.1
707 Mlawer EJ, Taubman SJ, Brown PD, et al. (1997) Radiative transfer for inhomogeneous
708 atmospheres: RRTM, a validated correlated-k model for the longwave. J Geophys
709 Res-Atmos 102:16663–16682. doi: 10.1029/97JD00237
710 Monin AS, Obukhov Am (1954) Basic laws of turbulent mixing in the surface layer of
711 the atmosphere. Contrib Geophys Inst Acad Sci USSR 151:163–187.
712 Mulitza S, Prange M, Stuut JB, et al. (2008) Sahel megadroughts triggered by glacial
713 slowdowns of Atlantic meridional overturning. Paleoceanography. doi:
714 10.1029/2008PA001637
715 Nicholson S (1979) Revised Rainfall Series for the West-African Subtropics. Mon
716 Weather Rev 107:620–623. doi: 10.1175/1520-
717 0493(1979)107<0620:RRSFTW>2.0.CO;2
718 Nicholson S (2009) On the factors modulating the intensity of the tropical rainbelt over
719 West Africa. Int J Clim 29:673–689. doi: 10.1002/joc.1702
720 Niedermeyer EM, Prange M, Mulitza S, et al. (2009) Extratropical forcing of Sahel
721 aridity during Heinrich stadials. Geophys Res Lett. doi: 10.1029/2009GL039687
722 Patricola CM, Cook KH (2008) Atmosphere/vegetation feedbacks: A mechanism for
723 abrupt climate change over northern Africa. J Geophys Res-Atmospheres. doi:
724 10.1029/2007JD009608

725 Patricola CM, Cook KH (2010) Northern African climate at the end of the twenty-first
726 century: an integrated application of regional and global climate models. Clim Dyn
727 35:193–212. doi: 10.1007/s00382-009-0623-7
728 Rotstayn LD, Lohmann U (2002) Tropical rainfall trends and the indirect aerosol effect. J
729 Clim, 15(15), pp.2103–2116.
730 Rowell DP, Folland CK, Maskell K, Ward MN (1995) Variability of summer rainfall
731 over tropical north-africa (1906-92) observations and modeling. Q J R Meteorol Soc
732 121:669–704. doi: 10.1256/smsqj.52310
733 Shanahan T, Overpeck J, Anchukaitis K, et al. (2009) Atlantic Forcing of Persistent
734 Drought in West Africa. Science 324:377–380. doi: 10.1126/science.1166352
735 Shell K, Kiehl J, Shields C (2008) Using the radiative kernel technique to calculate
736 climate feedbacks in NCAR's Community Atmospheric Model. J Clim 21:2269–
737 2282. doi: 10.1175/2007JCLI2044.1
738 Skamarock WC, Klemp JB, Dudhia J, et al. (2008) A description of the Advanced
739 Research WRF Version 3. NCAR/TN-475+ STR
740 Smirnova TG, Brown JM, Benjamin SG (1997) Performance of different soil model
741 configurations in simulating ground surface temperature and surface fluxes. Mon
742 Weather Rev 125:1870–1884. doi: 10.1175/1520-
743 0493(1997)125<1870:PODSMC>2.0.CO;2
744 Soden B, Held I, Colman R, et al. (2008) Quantifying climate feedbacks using radiative
745 kernels. J Clim 21:3504–3520. doi: 10.1175/2007JCLI2110.1

746 Stager J, Ryves D, Chase B, Pausata F (2011) Catastrophic Drought in the Afro-Asian
747 Monsoon Region During Heinrich Event 1. Science 331:1299–1302. doi:
748 10.1126/science.1198322
749 van Kreveld S, Sarnthein M, Erlenkeuser H, et al. (2000) Potential links between surging
750 ice sheets, circulation changes, and the Dansgaard-Oeschger cycles in the Irminger
751 Sea, 60-18 kyr. Paleoceanography 15:425–442. doi: 10.1029/1999PA000464
752 Vellinga M, Wood R (2002) Global climatic impacts of a collapse of the Atlantic
753 thermohaline circulation. Clim Change 54:251–267. doi: 10.1023/A:1016168827653
754 Wang Y, Cheng H, Edwards R, et al. (2001) A high-resolution absolute-dated Late
755 Pleistocene monsoon record from Hulu Cave, China. Science 294:2345–2348.
756 Xue Y and Jagadish S (1993) The influence of land surface properties on Sahel climate.
757 Part 1: desertification. J Clim, 6(12), pp.2232–2245.
758 Zhang R, Delworth TL (2005) Simulated tropical response to a substantial weakening of
759 the Atlantic thermohaline circulation. J Clim 18:1853–1860.
760 Zhang G, Mcfarlane N (1995) Sensitivity of Climate Simulations to the Parameterization
761 of Cumulus Convection in the Canadian Climate Center General-Circulation Model.
762 Atmos-Ocean 33:407–446.
763 Zhou T, Yu R, Li H, Wang B (2008) Ocean forcing to changes in global monsoon
764 precipitation over the recent half-century. J Clim 21:3833–3852.

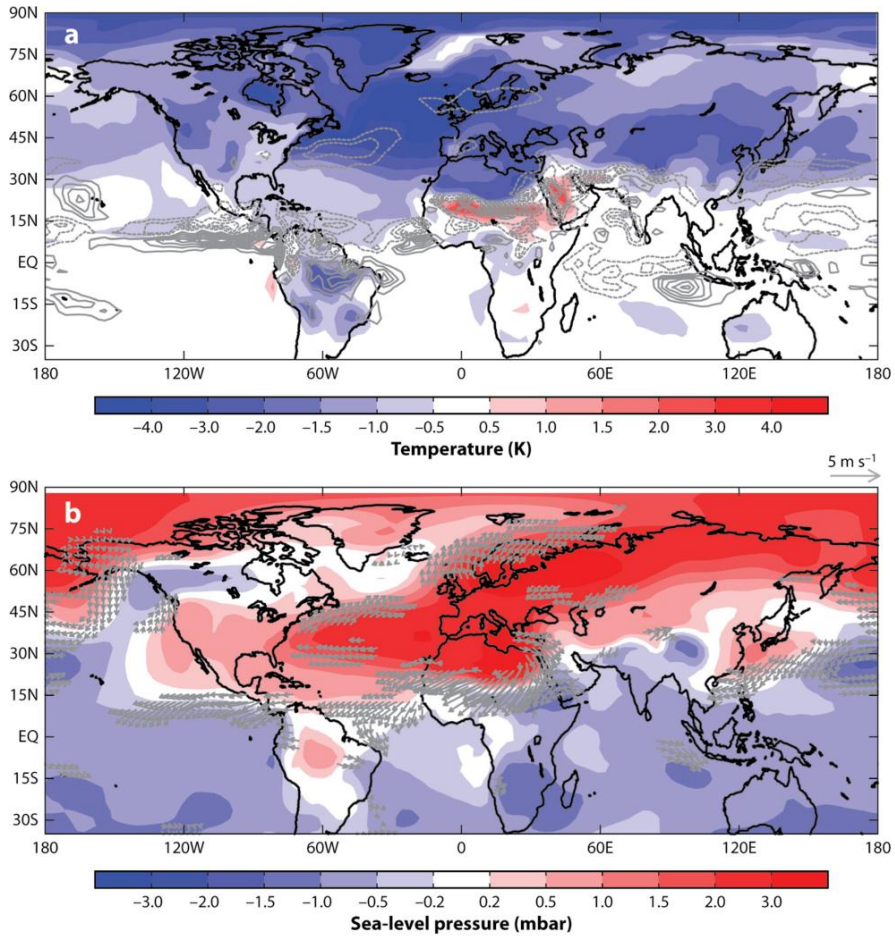

766

767 **Fig. 1** July through September anomalies from a Community Atmosphere Model 3–slab

768 ocean simulation, where a 30 W m^{-2} cooling is applied to the slab ocean in the

769 midlatitude North Atlantic. Both control and cooling simulations were 30 years long, and

770 the anomalies are derived from the last 20 years. (a) Temperature (shaded; K) and

771 precipitation (gray contour; interval is 0.5 mm per day, and dashed lines are negative). (b)

772 Sea-level pressure (shaded; millibars) and lowest-level wind anomalies (reference vector

773 is 5 m s^{-1}; only anomalies exceeding 1 m s^{-1} in magnitude shown). The images show the

774 hemispheric impact of North Atlantic cooling and resulting modification of the tropical

775 circulation. Adopted from Chiang and Friedman (2012)

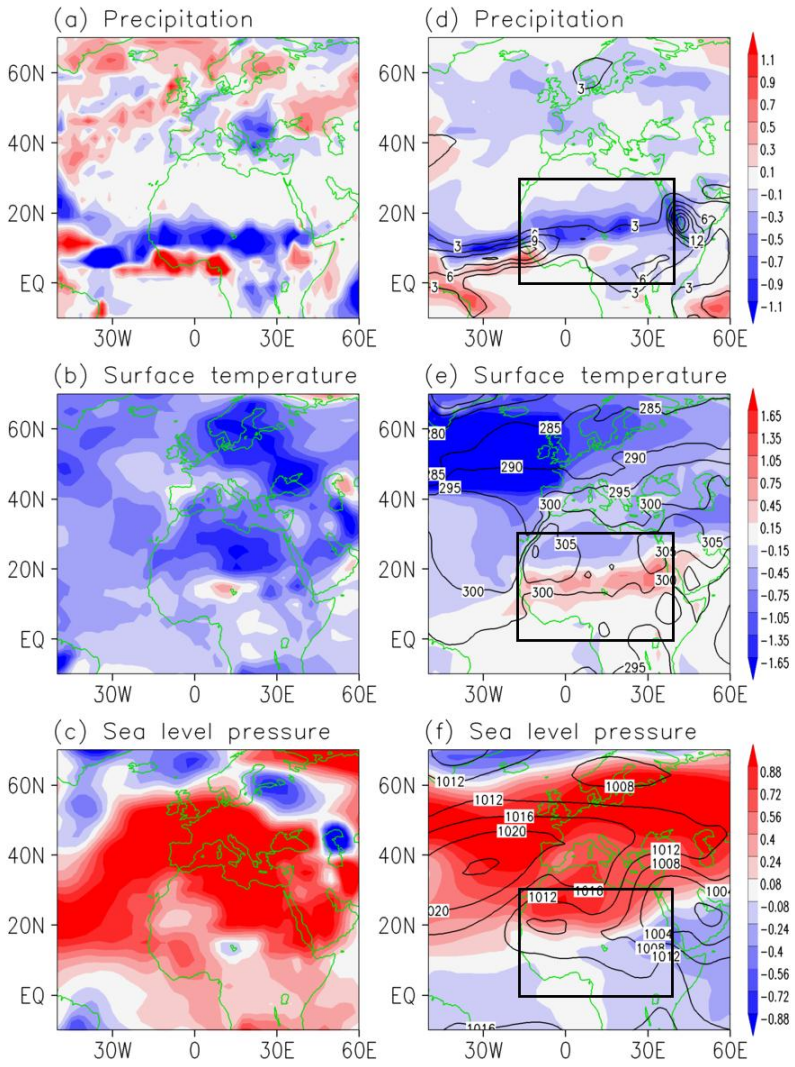

776

777 **Fig. 2** July through September averaged precipitation (upper panels; mm/day), surface
778 temperature (middle panels; K) and sea level pressure (lower panels; hPa). Left column:
779 difference of observed precipitation and reanalysis surface temperature and SLP between
780 Sahara cold years (1979, 1981, 1984, 1985, 1992, 1993, 1996-1997) and Sahara warm
781 years (1998-1999, 2001-2003, 2005-2006, 2008). Right column: control run (contour)
782 and anomalies in the cooling minus control run (shading), in the AGCM simulation using
783 CAM3.5 coupled with a slab ocean model with 2K cooling prescribed in between 45 °-

784 60 °over North Atlantic. Both observation and model simulation show Sahel rainfall
785 reduction, and broad cooling and a SLP increase over Sahara. The color bar for each row
786 is relevant to both panels of the row. The black box denotes the plotted domain of WRF
787 simulation in Fig. 5a-5c. Observations and reanalysis data source: precipitation, GPCP
788 combined precipitation data, developed and computed by the NASA/Goddard Space
789 Flight Center's Laboratory for Atmospheres as a contribution to the GEWEX Global
790 Precipitation Climatology Project (Adler et al. 2003); Surface temperature and SLP:
791 NCEP/NCAR Reanalysis 1 (Kalnay et al. 1996).

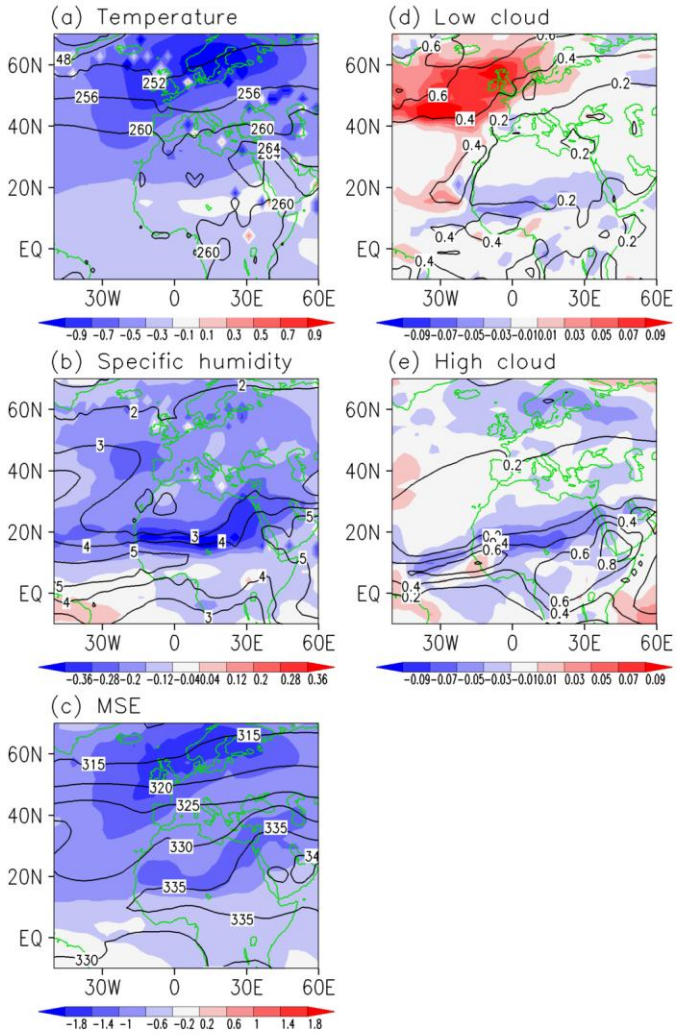

792

793 **Fig**. **3** July through September averaged (a) mean tropospheric temperature (K), (b) mean

794 tropospheric specific humidity (g/kg), (c) mean tropospheric moist static energy (kJ), (d)

795 low cloud coverage (fraction) and (e) high cloud coverage (fraction) in the CAM3.5

796 simulation for both the control run (contour) and anomalies in the cooling minus control

797 run (shading)

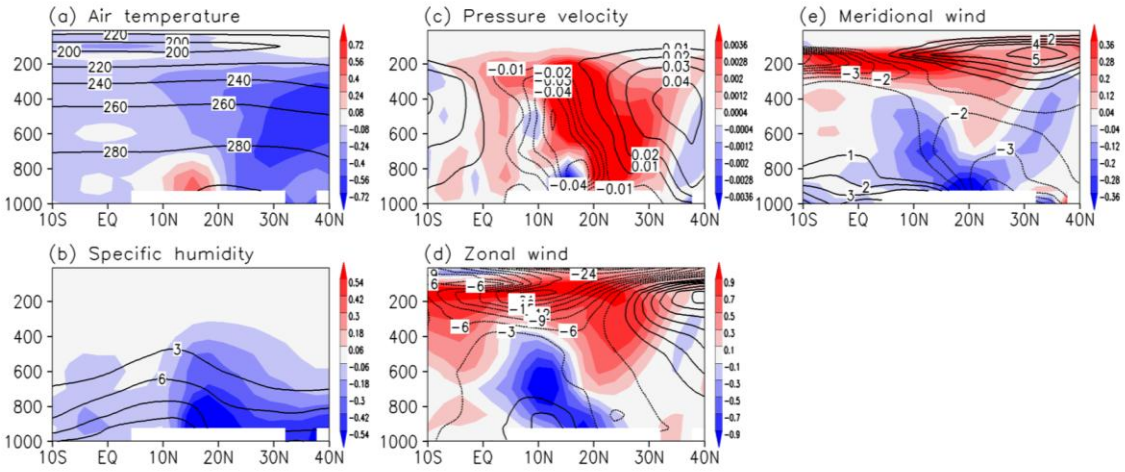

798

799 **Fig**. **4**. Same as Fig. 3 but for pressure-level vertical profile of (a) air temperature (K), (b)

800 specific humidity (g/kg), (c) pressure velocity (Pa/s), (d) zonal wind (m/s) and (e)

801 meridional wind (m/s). All fields are averaged between 10 ℃W and 30 ℃E. Regions of no

802 data (topography) are left blank.

803

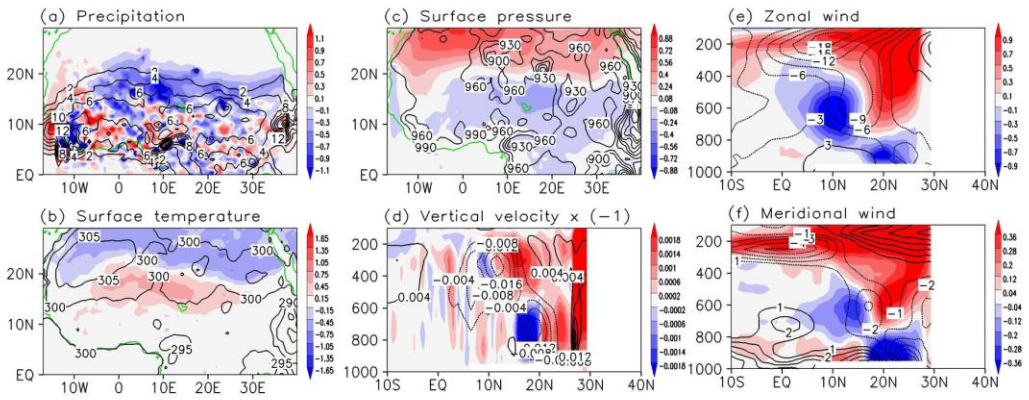

Fig. 5. July-August averaged climate over Africa for the control run (contour) and anomalies in the experiment (shading) of the WRF simulation with temperature, geopotential height and relative humidity anomalies from the AGCM cooling runs forced at the northern boundary of the domain. (a) – (c), surface fields: (a) precipitation (mm/day), (b) surface temperature (K) and (c) surface pressure (hPa). Only portion of the domain north of the equator is shown for clarity. (d) – (f), pressure-level vertical profile of wind component: (d) vertical velocity (multiplied by -1 in accordance with the sign of pressure vertical velocity; m/s), (e) zonal wind (m/s) and (f) meridional wind (m/s). All vertical profiles are averaged from 10 °W to 30 °E and the plots are extended to 40 ℃N to have the same scale as in Fig. 4. Regions of no data (topography and north of 30 ℃N in the plots for vertical profiles) are blank. The WRF cooling simulation generally simulates the Sahel rainfall reduction, and associated temperature, pressure, and circulation changes as in the GCM.

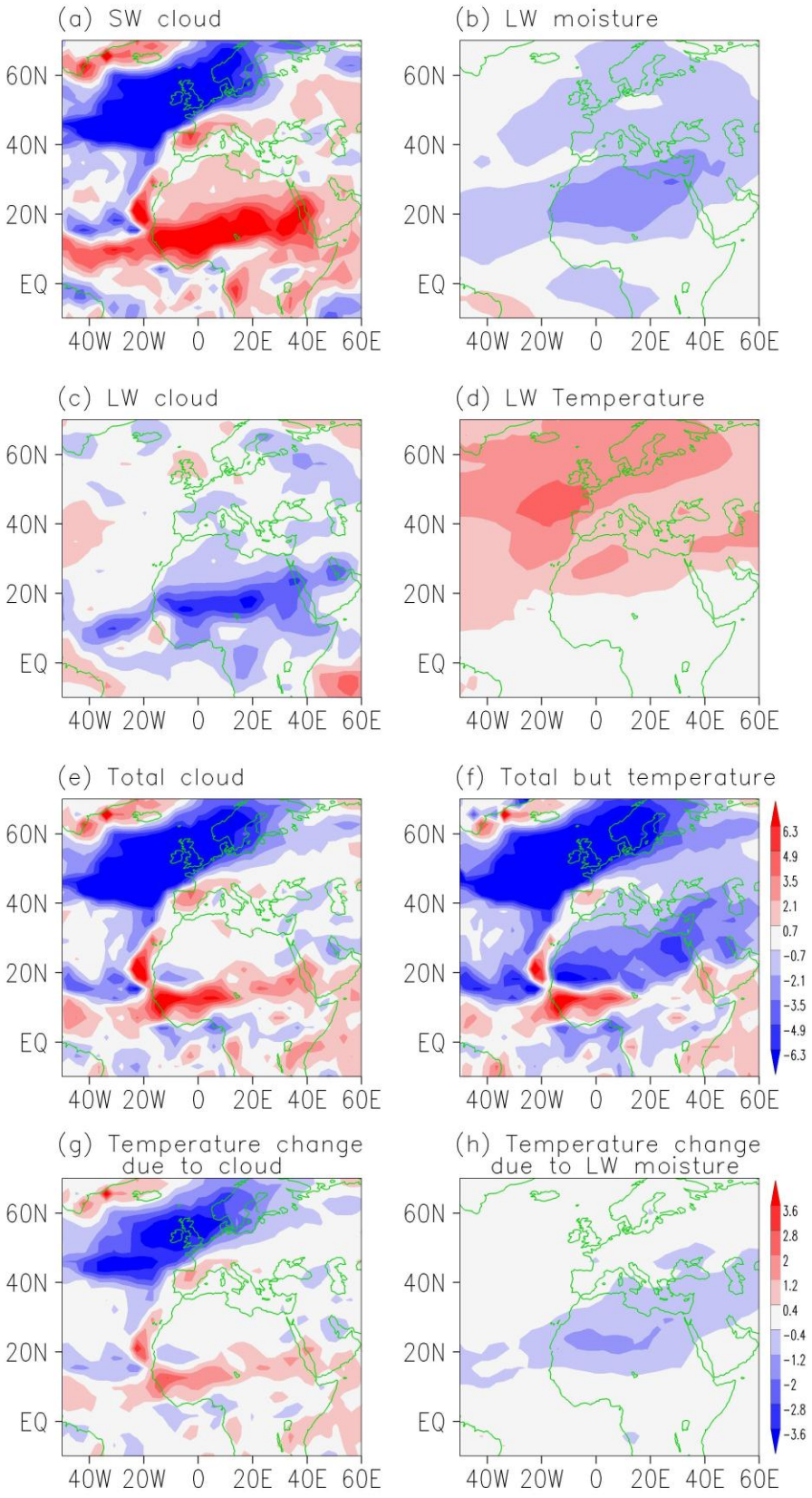
(a) SW cloud
(b) LW moisture
(c) LW cloud
(d) LW Temperature
(e) Total cloud
(f) Total but temperature
(g) Temperature change due to cloud
(h) Temperature change due to LW moisture
60N
40N
20N
EQ
40W 20W 0 20E 40E 60E
6.3
4.9
3.5
2.1
0.7
-0.7
-2.1
-3.5
-4.9
-6.3
3.6
2.8
2
1.2
0.4
-0.4
-1.2
-2
-2.8
-3.6

818

819 **Fig**. **6** July through September average of TOA Energy flux anomalies due to the
820 feedback of (a) cloud shortwave, (b) moisture longwave, (c) cloud longwave, (d) surface
821 and air temperature longwave, (e) total cloud and (f) total with the exception of
822 temperature, and of partial temperature anomalies due to (g) total cloud feedback and (h)
823 longwave moisture feedback, in the CAM3.5 simulation. The color bar for (a) – (f) is to
824 the right of panel (f), and for (g) – (h) is to the right of panel (h). The units for (a) – (f)
825 are W m^{-2} and for (g) – (h) are K. The figures show that positive cloud (moisture)
826 feedbacks strongly augment the cooling in extratropics (tropics)

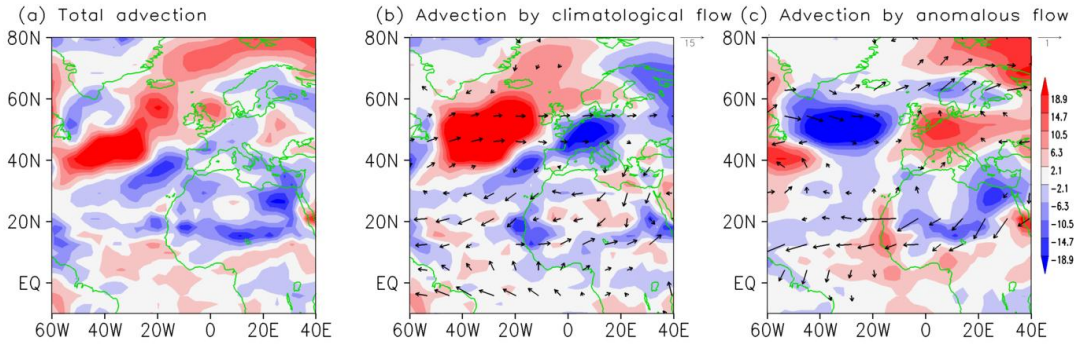

827

828 **Fig**. **7** July through September average of vertically integrated horizontal MSE advection

829 anomalies in the CAM3.5 simulation (unit: W m^{-2}). (a) total anomaly, (b) the anomaly

830 related to the climatological flow from the control run, (c) the anomaly related to

831 anomalous flow. Arrows are 925mb mean flow (b) and anomalous flow (c) (unit: m/s).

832 The figure shows that the advection of low MSE air cools North Africa.

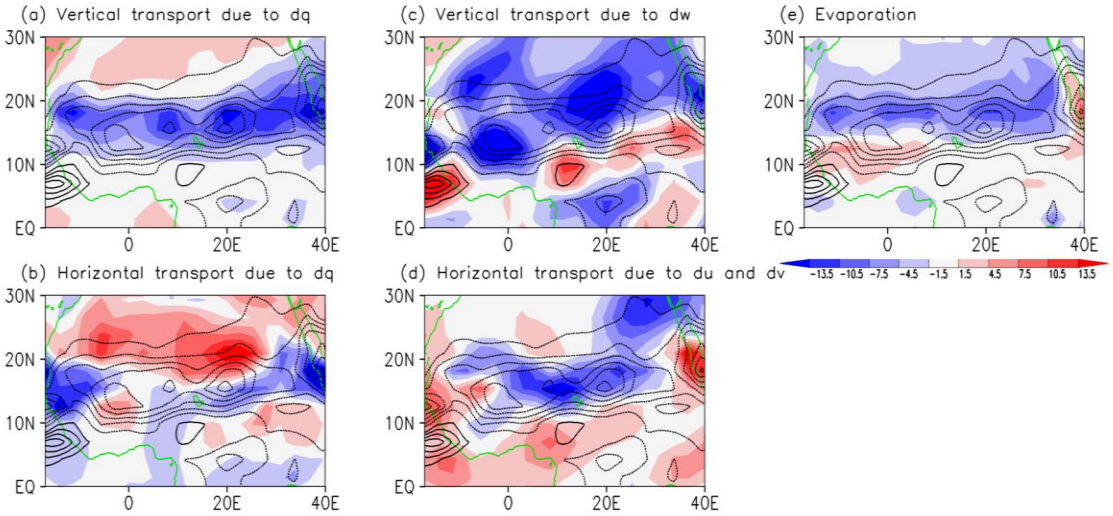

833

834 **Fig**. **8** July through September average of vertically-integrated moisture budget

835 anomalies in the CAM3.5 simulation. Contour: total precipitation anomaly. Shading: (a)

836 vertical moisture transport anomaly due to anomalous moisture, (b) horizontal moisture

837 transport anomaly due to anomalous moisture, (c) vertical moisture transport anomaly

838 due to anomalous vertical wind, (d) horizontal moisture transport anomaly due to

839 anomalous horizontal wind and (e) evaporation anomaly. The unit is W m^{-2}. Contour

840 interval: 5 W m^{-2}. The color bar for all panels is at the bottom of panel (e)